Acta Acustica 2026, **10**, 74

https://doi.org/10.1051/aacus/2026068

Topical Issue - Benchmarking Problems and Datasets in Acoustics

Available online at:
https://acta-acustica.edpsciences.org

TECHNICAL & APPLIED ARTICLE

OPEN ACCESS

FLOW-01: A benchmark dataset for aerodynamic noise and wake flow fields generated by circular cylinders in a crossflow

Thomas F. Geyer[1,*], Paul Abromeit[2], and Stefan Schoder[3]

[1]Institute of Electrified Aero Engines, German Aerospace Center (DLR e.V.), Lieberoser Str. 13A, 03046 Cottbus, Germany
[2]Brandenburg University of Technology Cottbus - Senftenberg (BTU), Chair of Electrified Aero Engines, Lieberoser Str. 13A, 03046 Cottbus, Germany
[3]Institute of Fundamentals and Theory in Electrical Engineering (IGTE), Graz University of Technology, Inffeldgasse 18/I, 8010 Graz, Austria

Received 21 January 2026, Accepted 27 June 2026

Abstract – Aeroacoustic measurements and numerical predictions are commonly used to determine the sound generation from fluid flows. This work documents the measurement of the aerodynamic sound generation by a circular cylinder in crossflow. Three different velocities are studied, and based on the experimental data, a simplified aeroacoustic sound prediction workflow is presented to estimate the radiated far-field noise. The experimental dataset and the numerical simulation setup in open-source software packages are provided online. The geometrical and flow definitions, along with the experimental dataset, constitute a standardised configuration (called `FLOW-01`) proposed as a validation benchmark for numerical simulation workflows and as a reference for the design of measurement facilities. A strongly simplified 2D numerical simulation using OpenFoam and openCFS is provided with the emphasis to run on a typical personal computer hardware. As a consequence, the provided numerical simulation of the flow is not resolving the turbulent structures nor the 3D characteristics of the flow which are known from experimental and numerical studies.

Keywords. Benchmark, Dataset, Cylinder, Crossflow, Vortex shedding

1 Introduction

The aerodynamic noise generated by a circular cylinder in crossflow is a classical problem in the field of aeroacoustics. It occurs in a large variety of technical applications, such as the pantograph of trains, the landing gear of aircraft as well as antennas and other protruding struts of vehicles. Consequently, much research has been dedicated to this problem, which includes experimental studies (see, for example, [1–5]) as well as analytical and numerical work [6–8].

This document describes acoustic and flow measurements on a set of two-dimensional circular cylinders of different diameter performed in an aeroacoustic wind tunnel as a benchmark case for numerical simulations. The acoustic measurements are a subset of the experiments described by Geyer [9] with additional wake flow measurements. In addition to the experimental dataset, 2D aeroacoustic simulations using the Perturbed Convective Wave Equation (PCWE) are provided as a reference workflow for aeroacoustic predictions.

*Corresponding author: `thomas.geyer@dlr.de`

2 Experimental setup

2.1 Wind tunnel

The experiments took place in the small aeroacoustic open jet wind tunnel at the Brandenburg University of Technology, which is described in detail in [10]. Figure 1 shows a schematic and a photograph of the experimental setup. The test section of the wind tunnel has dimensions of 2 m (streamwise) × 1.55 m (vertical) × 1.5 m (height). It is lined on five sides with a 0.25 m thick layer of absorbing melamine resin foam. Absorption coefficients taken from the manufacturers data sheet are presented in Figure 2 for different standard thicknesses. For absorber plates with an even greater thickness of 0.25 m, the absorption coefficient can be assumed to be above 0.9 even at lower frequencies, thus leading to a virtually anechoic environment for frequencies ≥125 Hz. For the experiments, a wind tunnel nozzle with a rectangular exit area with dimensions of 0.23 m × 0.28 m was used, which allows for flow velocities up to approximately 50 m/s. Attached to the nozzle were two side plates made of acrylic glass, to which the cylinder models were mounted. These plates have a streamwise

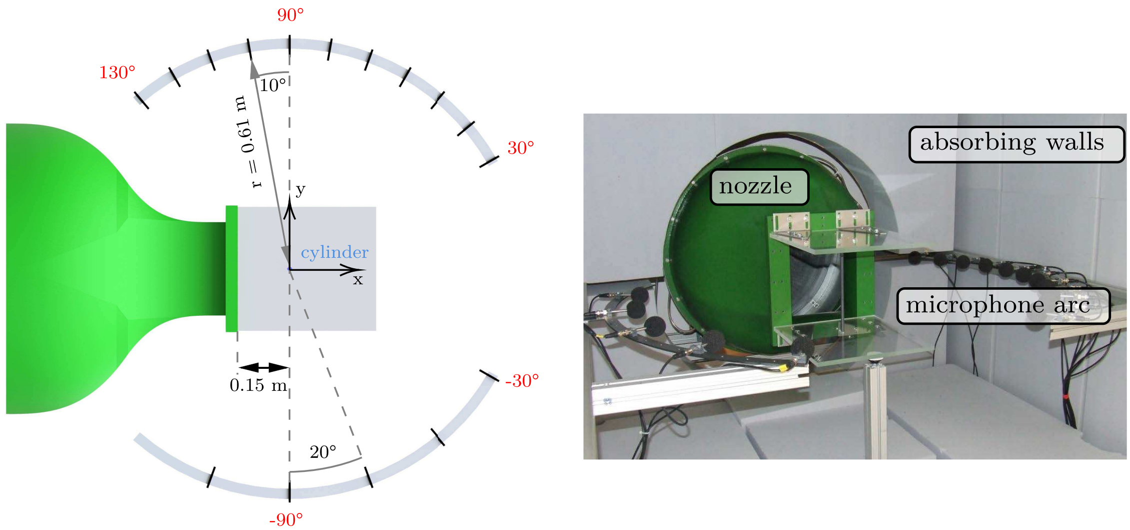

(a) Schematic (top view) (b) Photograph

Figure 1. Experimental setup in the aeroacoustic wind tunnel.

length of 0.4 m and a horizontal length of 0.38 m. In this setup, the x-axis is aligned with the streamwise direction, the y-axis is aligned with the horizontal direction and the z-axis is aligned with the cylinder span.

In the experiments, selected velocities were adjusted by adjusting the pressure in the settling chamber of the wind tunnel. From the total set of measurements, acoustic time data are provided for three velocities U_0, corresponding to Mach numbers $M = U_0/c$ (with c being the speed of sound) from approximately 0.08 to 0.15. They are specified in Table 1. Please note that the Mach numbers in the table were calculated for a nominal temperature of 20 °C. The correct temperature in the wind tunnel test section was obtained for each measurement series and is specified for each acoustic data set.

The corresponding turbulence intensity at these flow velocities is also specified, using data from a study that was done with the same experimental setup [12]. In that study, measurements of the inflow turbulence were made at 10 positions randomly distributed in a plane normal to the flow in a downstream distance of 0.15 m from the nozzle exit, without the cylinder in place. The results are shown in Figure 3. As the maximum velocity in that study was only 35 m/s, the turbulence intensity at the highest flow speed of the current benchmark was linearly extrapolated. It can be seen from Table 1 that the turbulence intensity at the location of the cylinders is below 0.3%.

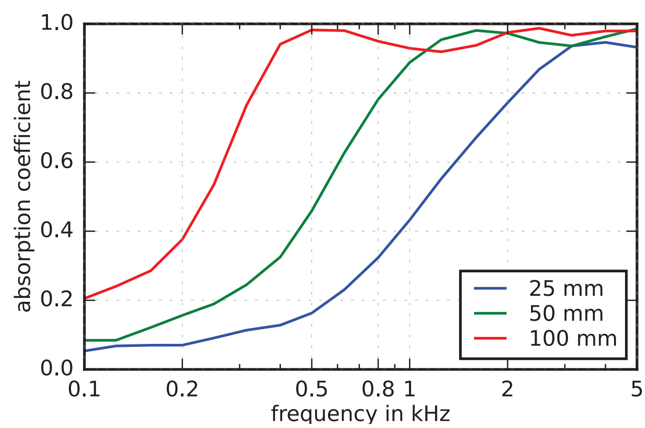

Figure 2. Absorption coefficients of the material with which the wind tunnel test section is lined, taken from the data sheet for different standard thicknesses [11].

Table 1. Velocities adjusted in the experiments.

Velocity U_0 (m/s)	Mach number $M = U_0/c$	Turbulence intensity Tu (%)
25.8	0.075	0.27
36.5	0.106	0.27
49.9	0.146	0.29

2.2 Cylinder models

This benchmark contains data obtained for five two-dimensional circular cylinders with diameters between 6 mm and 30 mm. They were made of either aluminum (for the 6 mm cylinder) or polyurethane (all remaining cylinders). Their dimensions are given in Table 2. It can be seen that the aspect ratio is >7 for all cylinders so that periodic von-Kármán vortex shedding can be expected [13].

Inserting a bluff body into a finite-sized wind tunnel test section leads to blockage, the values of which are also included in Table 2. It is known that a wind tunnel blockage of up to 10% only has a negligible effect (see, for example, [14]), which is true for nearly all cylinders of the present study. The only exception is the cylinder with a diameter of 30 mm, for which the blockage ratio is 13%. In order to account for this blockage effect, different correction methods are available, such as a simple velocity correction provided in [15]. For the present data

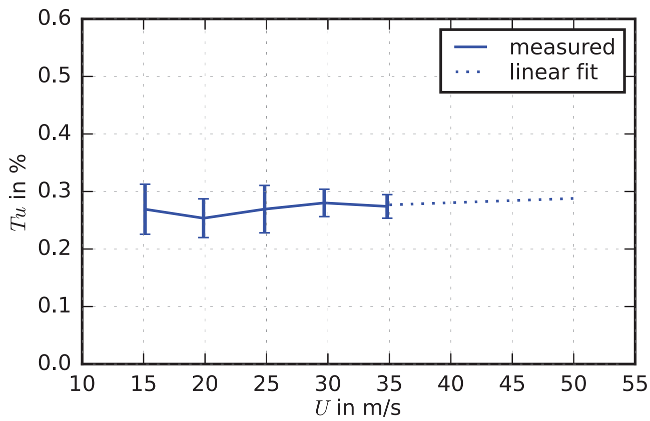

Figure 3. Turbulence intensity in a downstream distance of 0.15 m from the nozzle exit (taken from [12] and extrapolated for the current velocity range).

set, this correction would lead to a maximum increase in velocity of about 1.6 m/s (corresponding to an increase in Mach number of about 3.3%). Still, it is worth mentioning that for circular cylinders, the effect of blockage on the resulting vortex shedding Strouhal number is very minor only for blockage ratios of up to 20% [16]. In addition, it should be noted that such a simple correction method may not be able to fully account for the more or less three-dimensional flow field encountered by the cylinders in the present setup. Due to these reasons, the velocities have not been corrected in the current paper and in the benchmark dataset.

In addition to the cylinder noise data, acoustic data is provided for the wind tunnel background noise, and hence without a cylinder placed inside the test section.

The resulting Reynolds numbers corresponding to the velocities from Table 1 based on the cylinder diameters from Table 2 are in a range from approximately 10,000 to 100,000. This range belongs to the subcritical flow regime, where transition happens along the free shear layers [3].

2.3 Acoustic measurements

In [9], acoustic measurements were performed with 16 microphones arranged on two arcs positioned on opposite sides of the wind tunnel test section (see Fig. 1). The microphones are Class 1 ICP 1/4th-inch free field microphones type MI-17 with a nominal sensitivity of 50 mV/Pa and a typical frequency response of ±0.5 dB for frequencies between 20 Hz and 4 kHz. The microphones were calibrated at a single frequency of 1 kHz using a Class 2 calibrator with an amplitude of 94 dB (1 Pa).

In this benchmark, data are provided for microphones located at a distance of 0.61 m at angles from 40° to 130° to the flow. Sound pressures were recorded using a National Instruments 24 Bit multichannel measurement system with a sampling frequency of 51.2 kHz and a duration of 90 s. The complete time series are provided in this benchmark.

It should be noted that for acoustic measurements at increasing flow speeds, it is common to account for the effect of refraction of sound at the wind tunnel shear layers (see, for example, [17–20]). However, due to the relatively low Mach numbers in the present experiments and the fact that the distance covered by the acoustic waves inside the wind tunnel core jet ($\lessapprox$0.1 m for the microphone located at 90° to the flow) is much smaller than the total distance (0.61 m), no correction was applied.

Table 2. Cylinders used in the experiments.

Diameter d (mm)	Length l (mm)	Aspect ratio l/d	Blockage (%)
6	280	46.7	2.6
10	280	28	4.3
13	280	21.5	5.6
20	280	14	8.7
30	280	9.3	13.0

2.4 Flow field measurements

In addition to the acoustic measurements, Constant Temperature Anemometry (CTA) measurements were performed in the wake of the cylinder models for a single velocity of 36.5 m/s ($M = 0.106$). This was done using a Dantec P11-type single wire miniature probe, which consists of a platinum–plated tungsten wire sensor with a diameter of 5 μm and a length of 1.2 mm, and a Dantec multichannel CTA measurement system. This system contains a hardware low–pass filter with a cutoff frequency of 10 kHz. Velocity calibration of the hot-wire probe was performed against a vane anemometer with an accuracy of ±0.2 m/s/±2% and a measurement range of 0.4 m/s to 40 m/s using a 4th order polynomial curve fit. The polynomial curve fit is known to give linearization errors of less than 1% [21]. The probe was traversed along a line normal to the cylinder axis and to the direction of the flow (along the y-direction, see Fig. 1a) in a distance of one cylinder diameter d downstream from the cylinder axis through the wake. Due to the expected symmetry of the wake flow region, only one half of the wake region was covered. The probe was traversed using a three-dimensional traverse system made by Isel Germany GmbH with a minimum step size of 0.1 mm and a repeat accuracy of ±0.02 mm. The grid resolution was increased from 0.2 mm directly downstream of the cylinder to 0.5 mm. However, the flow data presented as part of this benchmark are given with a uniform grid spacing of 0.5 mm, obtained by applying a spline fit to the measured wake profiles.

The data were recorded with a sampling frequency of 25.6 kHz and a measurement duration of 10 s per measurement point using a 24 Bit data acquisition module. In addition, the temperature was corrected based on simultaneous measurements with a Dantec P90-type temperature probe. In post-processing, the first second of each data set was omitted in order to remove the possible effect of vibrations of the probe after each step of the traverse system. From the remaining 230 000 samples, the mean value U as well as the rms-value $\tilde{u}$ were calculated.

3 Experimental data description

3.1 Acoustic data

The results from the acoustic measurements are given as sound pressures in Pa, recorded by the microphones located at angles of 40° to 130° to the flow. They are stored as csv-files containing the (calibrated) pressure-time series.

Thereby, one separate csv-file was created for each cylinder and the background noise measurement at each flow velocity adjusted. Each file contains ten columns, one for each microphone (starting from the one at 40° to the one at 130° as shown in Figure 1a, upper arc), and 4.608.000 rows, corresponding to 90 s of the measured time signal with a time step of $\Delta t = 1/51200\,\text{s} = 19.5313\,\mu\text{s}$.

Thus, the following files are available containing the acoustic data:

– "soundpressure_6mm_diameter_M0074.csv" (for a Mach number of 0.074), "soundpressure_6mm_diameter_M0105.csv" (for a Mach number of 0.105), and "soundpressure_6mm_diameter_M0144.csv" (for a Mach number of 0.144), which contain 90 s of time data for ten microphones from 40° to 130° to the flow, temperature 25.4°C;
– "soundpressure_10mm_diameter_M0075.csv" (for a Mach number of 0.075), "soundpressure_10mm_diameter_M0106.csv" (for a Mach number of 0.106), and "soundpressure_10mm_diameter_M0145.csv" (for a Mach number of 0.145), which contain 90 s of time data for ten microphones from 40° to 130° to the flow, temperature 21.1°C;
– "soundpressure_13mm_diameter_M0074.csv" (for a Mach number of 0.074), "soundpressure_13mm_diameter_M0105.csv" (for a Mach number of 0.105), and "soundpressure_13mm_diameter_M0144.csv" (for a Mach number of 0.144), which contain 90 s of time data for ten microphones from 40° to 130° to the flow, temperature 27.3°C;
– "soundpressure_20mm_diameter_M0075.csv" (for a Mach number of 0.075), "soundpressure_20mm_diameter_M0106.csv" (for a Mach number of 0.106), and "soundpressure_20mm_diameter_M0145.csv" (for a Mach number of 0.145), which contain 90 s of time data for ten microphones from 40° to 130° to the flow, temperature 22.5°C;
– "soundpressure_30mm_diameter_M0074.csv" (for a Mach number of 0.074), "soundpressure_30mm_diameter_M0105.csv" (for a Mach number of 0.105), and "soundpressure_30mm_diameter_M0144.csv" (for a Mach number of 0.144), which contain 90 s of time data for ten microphones from 40° to 130° to the flow, temperature 26.0°C;
– "soundpressure_background_M0074.csv" (for a Mach number of 0.074), "soundpressure_background_M0105.csv" (for a Mach number of 0.105), and "soundpressure_background_M0143.csv" (for a Mach number of 0.143), which contain 90 s of time data for ten microphones from 40° to 130° to the flow, temperature 28.0°C.

3.2 Flow data

The results from the wake measurements are given as velocities in m/s, measured one cylinder diameter downstream from each cylinder axis. They are stored as csv-files.

One separate csv-file was created for each cylinder. Each file contains three columns: The first column contains the vertical location in the wake (along the y-axis, see Fig. 1a, with $y = 0$ being the location directly downstream from the cylinder axis), the second one the mean flow velocity U (averaged over 9 s) and the third one the rms-value of the flow velocity $\tilde{u}$ (averaged over 9 s). The number of rows is different for each cylinder, as the width of the half-wake was set to 3.5 times the cylinder diameter.

Thus, the following files are available containing the wake flow data:

– "wakeprofile_6mm_diameter.csv" (contains mean and rms-velocities at a nominal flow speed of 36.5 m/s for the cylinder with a diameter of 6 mm at a streamwise distance of 6 mm from the axis);
– "wakeprofile_10mm_diameter.csv" (contains mean and rms-velocities at a nominal flow speed of 36.5 m/s for the cylinder with a diameter of 10 mm at a streamwise distance of 10 mm from the axis);
– "wakeprofile_13mm_diameter.csv" (contains mean and rms-velocities at a nominal flow speed of 36.5 m/s for the cylinder with a diameter of 13 mm at a streamwise distance of 13 mm from the axis);
– "wakeprofile_20mm_diameter.csv" (contains mean and rms-velocities at a nominal flow speed of 36.5 m/s for the cylinder with a diameter of 20 mm at a streamwise distance of 20 mm from the axis);
– "wakeprofile_30mm_diameter.csv" (contains mean and rms-velocities at a nominal flow speed of 36.5 m/s for the cylinder with a diameter of 30 mm at a streamwise distance of 30 mm from the axis).

4 Experimental results

4.1 Experimental acoustic results

As a first example, Figure 4 shows sound pressure level spectra, obtained by performing an FFT using Welch's method [22] (Hanning window, block size 8192 samples, 50% overlap) on the time data provided for the microphone at 90° to the flow (column number 6 from each dataset provided). The amplitude was scaled by the frequency resolution to correspond to 1 $\mathrm{Pa}^2/\mathrm{Hz}$. The levels were calculated with a reference sound pressure p_0 of 20 μPa according to

$$L_p = 10 \log_{10} \left(\frac{p}{p_0} \right)^2 \text{ dB}. \quad (1)$$

The Mach numbers specified in the legend of each plot were calculated using the temperature-dependent speed of sound according to the estimation (see, for example, [23])

$$c(T) = 20.06 \sqrt{273.15 + T/(1°\mathrm{C})} \text{ m/s}, \quad (2)$$

with T being the temperature (in °C) provided with each dataset.

As a second example, Figure 5 shows the directivity of the vortex shedding tonal noise peak, obtained at all microphones from 40° to 130° on the upper arc shown in Figure 1a. The data from the microphone at 30° have been omitted, as it was found to be affected by the wind tunnel shear layer. It is visible that the noise radiated from the thinnest cylinder of the present study (6 mm diameter) differs from the expected classical dipole directivity, whereas this directivity is better visible for the cylinders with larger diameters (e.g., 30 mm).

4.2 Experimental flow results

Figure 6 shows half-profiles of the mean flow velocity and the rms-velocity, both normalized with the nominal flow speed of $U_0 = 36.5$ m/s, where $y/d = 0$ refers to the cylinder axis. These results can be generated using the experimental wake flow data provided in the benchmark.

In addition, Figure 7 shows corresponding spectra of the turbulent velocity fluctuations (in dB, relative to a reference velocity of 1 m/s), obtained from the hot-wire measurements in the wake of the cylinders. Basically, these results confirm the periodic vortex shedding, as the spectra show two clear peaks. The first appears at a Strouhal number (based on cylinder diameter) $St = f\,d/U_0$ around 0.2, which is known to be caused by fluctuations of the lift coefficient [1]. The second, weaker peak appears at twice that Strouhal number and is caused by fluctuating drag forces acting on the cylinder.

5 Aeroacoustic prediction

A 2D reference simulation setup (`simulation.zip`) for general purpose based on the perturbed convective wave equation (PCWE) [24, 25]

$$\frac{1}{c^2} \frac{\mathrm{D}^2 \psi^{\mathrm{a}}}{\mathrm{D}t^2} - \nabla \cdot \nabla \psi^{\mathrm{a}} = -\frac{1}{\bar{\rho} c^2} \frac{\mathrm{D} p^{\mathrm{ic}}}{\mathrm{D}t} \quad (3)$$

is presented using an open-source workflow based on `OpenFOAM`, `openCFS` [26] and `openCFS-Data` [27, 28] to simulate the flow-induced sound propagation. In equation (3), ψ^{a} denotes the acoustic velocity potential, c is the isentropic speed of sound, $\bar{\rho}$ represents the mean density, $\bar{\boldsymbol{v}}$ the mean fluid velocity, p^{ic} is the incompressible source pressure, and $\frac{\mathrm{D}}{\mathrm{D}t} = \frac{\partial}{\partial t} + \bar{\boldsymbol{v}} \cdot \nabla$ constitutes the material derivative. A 2D crossflow at a $d = 20$ mm diameter cylindrical bluff body is considered (with the dimensions of the experimental cylinders given in Tab. 2) at three Mach numbers (Ma = 0.075, 0.106, and 0.146, see Tab. 1) as a case study. Air at 20 °C is defined as the working medium. An unsteady flow field develops behind the bluff body, characterized by somewhat periodic vortex shedding at Strouhal numbers of 0.205 and 0.41 [4], which generates tonal components in the sound field. The Computational Fluid Dynamics (CFD) simulations were performed using `OpenFOAM`, and the incompressible pressure was used to compute the aeroacoustic sources based on the PCWE (e.g., [25, 29]) implemented in openCFS. These sources were then conservatively interpolated [30] onto the acoustic mesh, and acoustic propagation using the finite element method was subsequently computed with openCFS. The simulation workflow follows a structured directory hierarchy [31]:

- `0_mesh/`: Mesh files used by the simulations.
- `1_cfd/`: CFD setup of solver settings and initial flow fields.
- `2_sourceInterpolation/`: Interpolation of CFD results onto acoustic source regions.
- `3_ca/`: Acoustic propagation and SPL computation using Computational Aero Acoustics (CAA) solvers (e.g., PCWE [29]).
- `4_postprocessing/`: Plotting and data extraction.

This modular, hierarchical setup supports clarity, reproducibility, and automation across the aeroacoustic simulation pipeline. The simulation workflow is tailored to be executable on a typical notebook and not towards the latest accuracy of the results. Therefore, it can serve as a first aeroacoustic example for workshops to get in touch with the process and as a starting point for further modeling improvements as computational ressources allow it.

5.1 Aerodynamic simulation

The numerical investigation of the aerodynamics around the cylinder in a crossflow is conducted using the open-source finite-volume framework OpenFOAM (e.g., version 2412). The governing incompressible Navier–Stokes equations are solved on a structured computational grid, with the circular cylinder modelled as a quasi-two-dimensional object. No scale-resolved turbulence model is used for the simplified calculations, to allow a swift simulation on typical personal computer resources. The boundary conditions are prescribed by a uniform free-stream velocity at the inlet and a zero-pressure condition at the outlet. The cylinder surface is treated as a rigid, no-slip wall. The resulting pressure and velocity fields are stored in the EnSight format to facilitate

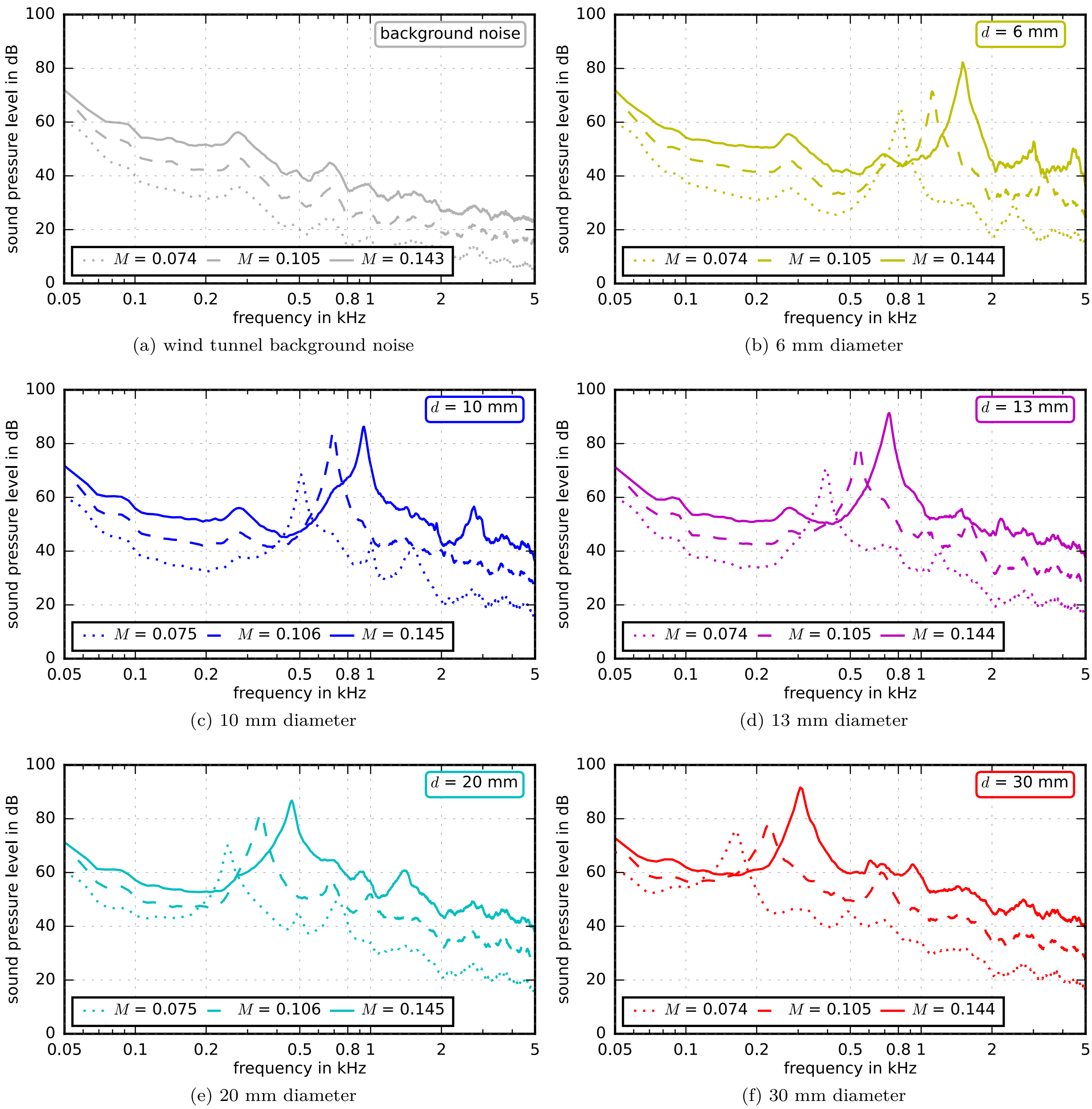

Figure 4. Sound pressure level spectra (re 20 μPa) obtained for the different cylinder models and the wind tunnel background noise at three flow velocities U_0 (amplitude scaled by frequency resolution).

subsequent analysis of the wake topology and aerodynamic force coefficients, such as drag and lift.

In accordance with the characteristic Strouhal number for this Reynolds number ($St \approx 0.2$), the fundamental vortex shedding frequency f is estimated as

$$f = St\frac{U_0}{d} \approx 250\text{–}500\,\text{Hz}. \tag{4}$$

To ensure sufficient temporal resolution for the acoustic analysis (e.g., for a Mach number $M = 0.075$), an acoustic signal sampling interval of $\Delta t_{\text{CA}} = 5 \cdot 10^{-4}\,\text{s} \approx \frac{1}{10f}$ was chosen. This sampling interval is the interval the field data is saved to the EnSight data exchange file for subsequent aerodynamic and aeroacoustic analysis.

The computational configuration and the aerodynamic simulation procedure are summarized as follows:

- **Mesh Generation:** Development of a structured computational grid optimized for the resolution of the boundary layer and wake regions.
- **Implementation of Boundary Conditions:**
  - **Inflow:** Uniform velocity $U_0 = 25.8\,\text{m/s}$ corresponding to $M = 0.075$.
  - **Outflow:** Static pressure-outlet with a prescribed value of zero.
- **Temporal Discretization and Solver Configuration:**

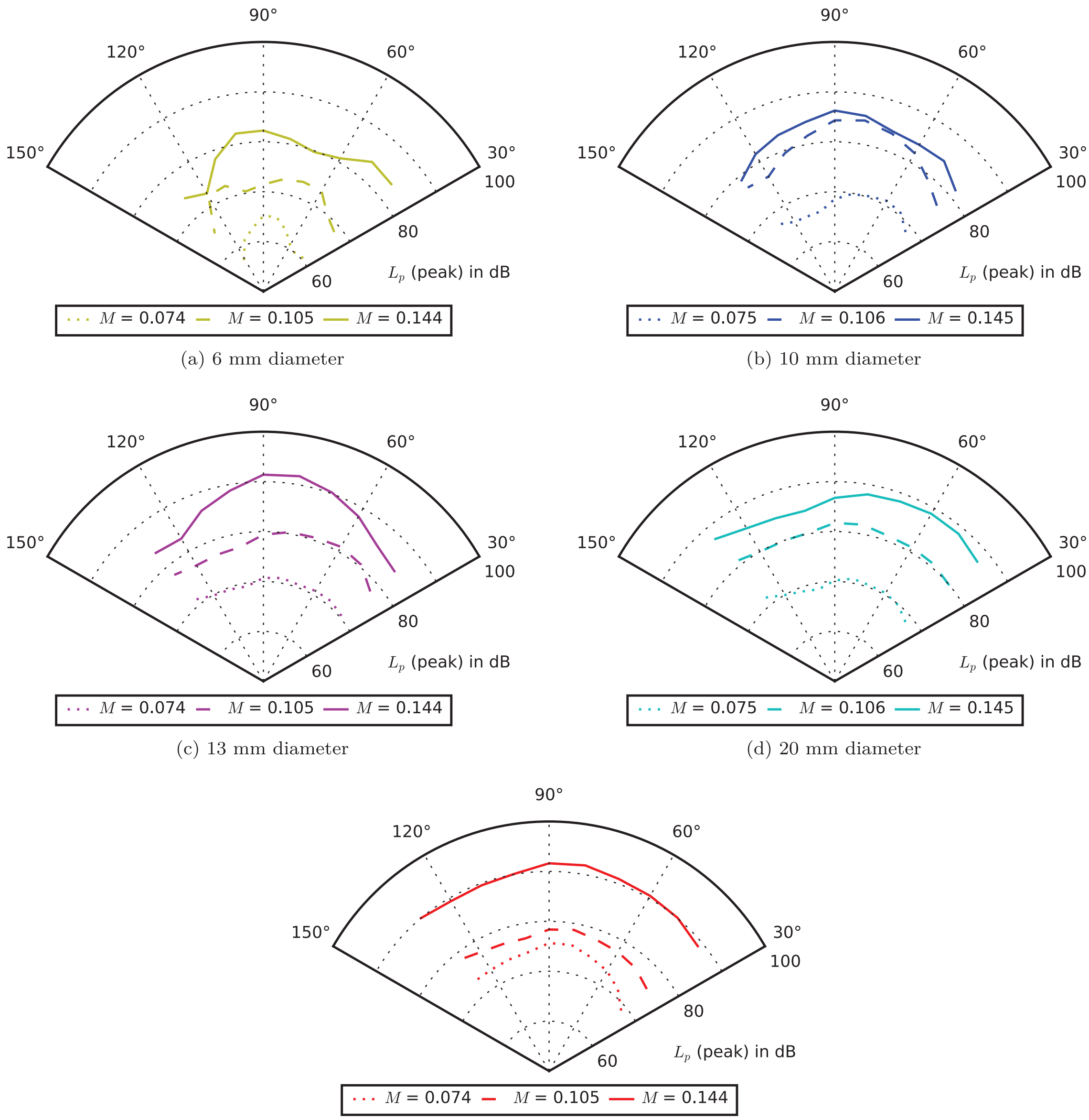

(a) 6 mm diameter (b) 10 mm diameter (c) 13 mm diameter (d) 20 mm diameter (e) 30 mm diameter

Figure 5. Sound pressure level directivities (re 20 μPa) obtained for the different cylinder models at three flow velocities U_0 (amplitude scaled by frequency resolution).

  - Integration time-step governed by the Courant–Friedrichs–Lewy (CFL) condition (CFL < 1), resulting in $\Delta t_{\mathrm{CFD}} = 4 \cdot 10^{-6}$ s.
  - Resolution of the transient flow via the *icoFoam* solver, employing the PISO (*Pressure-Implicit with Splitting of Operators*) algorithm for pressure-velocity coupling.
- **Convergence and Simulation Runtime:** Execution of the solver until a statistically steady-state vortex shedding oscillation is established.
- **Data Extraction and Interoperability:** Temporal pressure data are exported in the **EnSight Gold Case** format (`.case`) using the utility: (e.g., `foamToEnsight -fields ‘‘(‘p.’)’’ -time 0.5:1.3`)
  - This standardized CFD output format provides high interoperability.
  - The resulting datasets can be imported into ParaView for comparative analysis or visualization.

A similar setup can be derived using commercial third-party solvers (e.g., Star-CCM+, Ansys Fluent).

5.2 Source term processing

To compute the finite element methods right hand side

$$-\frac{1}{\bar{\rho} c^2} \int_\Omega \nu \frac{\mathrm{D} p^{\mathrm{ic}}}{\mathrm{D}t} \mathrm{d}\boldsymbol{x} \quad (5)$$

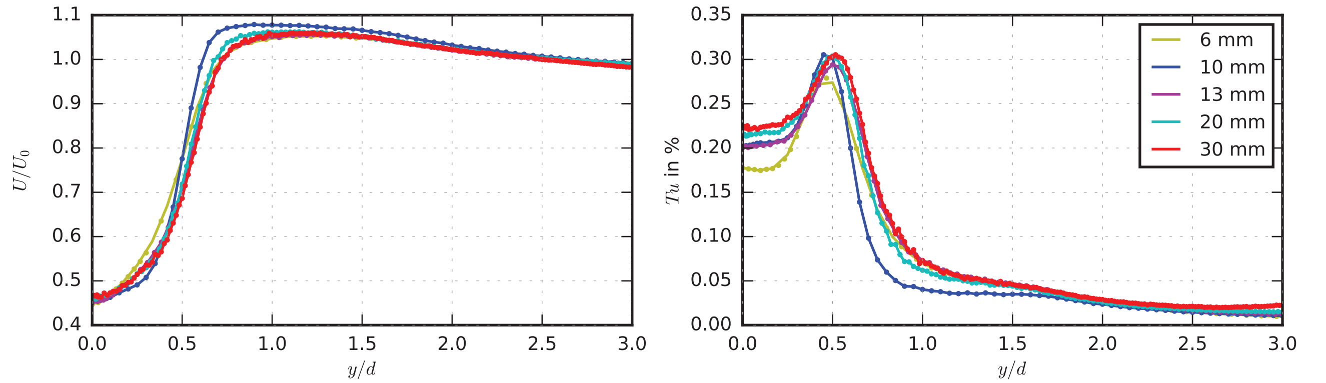

(a) Mean flow velocity

(b) Turbulence intensity

Figure 6. Flow (half-)profiles of the streamwise velocity component measured in the wake of the cylinders at a downstream distance of $1d$ from the cylinder axis at a nominal flow speed U_0 of 36.5 m/s ($M = 0.106$, markers: measured data, lines: spline fit).

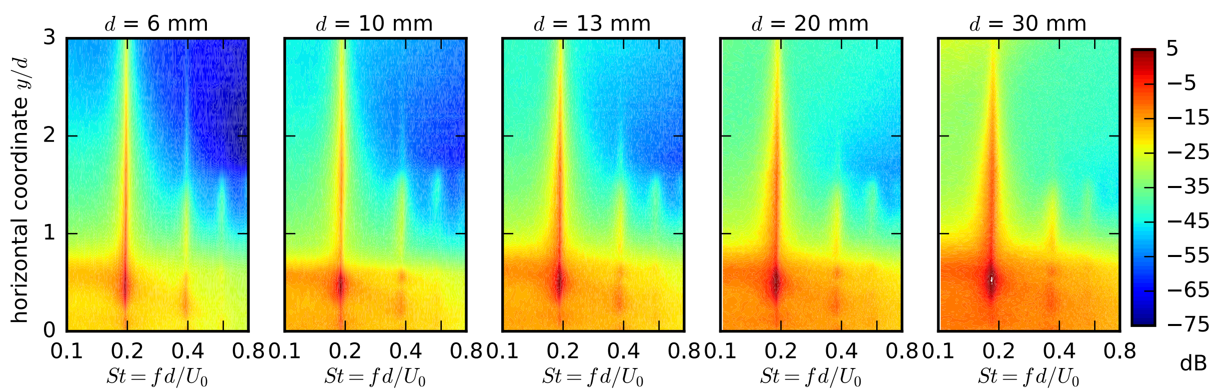

Figure 7. Spectral density of the fluctuating streamwise velocity component measured in the wake of the cylinders at a downstream distance of $1d$ from the cylinder axis at a nominal flow speed of 36.5 m/s ($M = 0.106$).

substantial derivative of the incompressible pressure $\frac{\mathrm{D}p^{\mathrm{ic}}}{\mathrm{D}t}$ needs to be computed. This involves several steps of the computation, reading the Ensight input data stored as a time series of the incompressible pressure in the time intervals of the acoustic simulation, the gradient of the incompressible pressure [32], the inner product of the pressure gradient and the mean velocity, the partial time derivative of the incompressible pressure field, adding them up to the substantial derivative of the incompressible pressure. After the calculation of the substantial derivative of the incompressible pressure, it is integrated onto the acoustic mesh by a conservative interpolation (for details, see [30]).

5.3 Acoustic simulation

The propagation of acoustic waves is modelled using the PCWE, which describes the sound field and frequency spectra in the presence of a background flow. The computational domain is truncated by a Perfectly Matched Layer (PML) to satisfy the free radiation condition and simulate an acoustic free-field. At the cylinder surface, a sound-hard boundary condition is enforced. The material properties of air are specified in the file *air.xml*. From the data, the speed of sound is computed as $c_0 \approx 343.5$ m/s. Within the source region of the acoustic simulation domain, the source term data are a result of a unsteady incompressible CFD simulation. Regarding the considered Mach number of the flow scenes $\mathrm{M} = \frac{U_0}{c_0} \approx \{0.075, 0.106, 0.146\} \ll 0.3$, the assumptions of the PCWE are satisfied. Furthermore, the influence of the convective term $\bar{\boldsymbol{v}} \cdot \nabla p^{\mathrm{ic}}$ on the right-hand side of the wave equation is negligible and is consequently omitted in this case [33]. The primary variable in this formulation (3) is the acoustic scalar potential ψ^{a}. The acoustic pressure can be computed by taking the material derivative of the scalar potential and scaling by the ambient density $p^{\mathrm{a}} = \rho_0 \frac{\mathrm{D}\psi^{\mathrm{a}}}{\mathrm{D}t}$ and consistently the acoustic particle velocity can be computed by $\boldsymbol{v}^{\mathrm{a}} = \nabla\psi^{\mathrm{a}}$.

The numerical simulation within the openCFS finite element framework[26] is structured according to the following procedure:

- **Input/Output Configuration:**
  - Specification of the computational mesh and unsteady right hand side source data for the finite element formulation.
  - Integration of the material property definitions (`air.xml`).

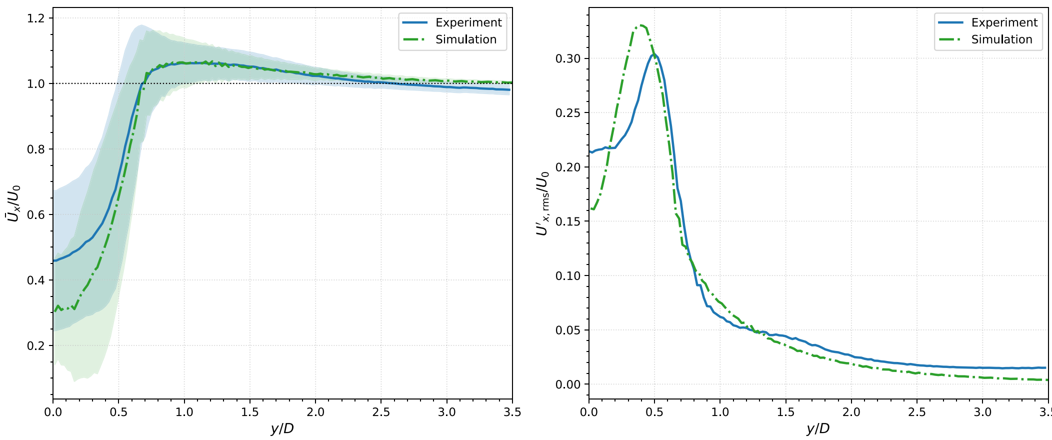

Figure 8. Validation of the flow (half-)profiles of the streamwise velocity component measured and simulated in the wake of the cylinders at a downstream distance of $1d$ from the cylinder axis at a nominal flow speed U_0 of 36.5 m/s ($M = 0.106$).

  - Definition of the output formats for post-processing and spectral analysis.
- **Domain Discretization and Setup:**
  - Assignment of material properties to the respective acoustic regions.
  - Definition of non-conforming interfaces using Nitsche-type mortaring to couple disparate mesh regions.
  - Placement of virtual microphones at coordinates for far-field evaluation.
- **Physics Definition and Solver Control:**
  - Selection of the transient analysis type for the acoustic simulation in openCFS.
  - Selection of the acoustic partial differential equation based on the acoustic potential as primary variable.
    - Definition of source regions and non-conforming interface coupling.
    - Application of damping coefficients for the PML buffer zones.
    - Integration of the mean flow field for the convective operator.
    - Prescription of the nodal source values, scaled by the factor $-\frac{1}{\rho_0 c_0^2}$.

Finally, the acoustic simulation can be run in parallel processes by the command-line `cfs -p propagation.xml -tX propagation` where **X** denotes the number of parallel threads utilized for the computation. As part of the aerodynamic simulation in OpenFoam [34], the Acoustic Analogy of Curle [35] is computed and provides an estimate of the aeroacoustic sound field in the observer point.

6 Simulation results

6.1 Aerodynamics

The aerodynamic data was validated by the mean and the root mean-squared values of the velocity at a downstream distance of $1d$ from the cylinder axis at a nominal flow speed U_0 of 36.5 m/s ($M = 0.106$). In the folder `postprocessing`, the Python 3 scripts is provided to obtain the resulting plot provided in Figure 8.

Despite the 2D simulation of the flow, fair agreement of the data was reached. However, these 2D results present a limited picture of the 3D turbulent flow structures of the cylinder wake.

6.2 Aeroacoustics

In the folder `postprocessing`, Python 3 scripts are provided to obtain the resulting plots provided in Figure 9. In the scripts, the experimental data is processed and this data handling can be used as example scripts for the experimental data usage. Furthermore, the python script shows how to handle the openCFS and OpenFoam exported history data (evaluation point history of the acoustic pressure). Since the acoustic pressure of the simulation in openCFS is modeled to be two-dimensional, the following corrections are applied to the simulation data: First the oscillation frequency is adapted to the one of a 3D cylinder (multiplied by the ratio of the respective Strouhal numbers 0.191/0.235). Secondly, the sound pressure level (SPL) in 3D

$$\mathrm{SPL_{3D}} = \mathrm{SPL_{2D}} + 10\log_{10}\left(\frac{\pi^2 r^2}{|H_0^{(1)}(kr)|^2}\right)\mathrm{dB} + 10\log_{10}\left(\frac{L_c}{L}\right)\mathrm{dB} \quad (6)$$

is computed from the 2D SPL value from the simulation. The second term is governed by the geometrical properties of the wave decay determined by the norm of the Green's function in 3D compared to the norm of the one in 2D.

It should be noted that no far field approximation of the Hankel function $H_0^{(1)}$ is possible since $kr \sim 1$, where k is the wave number and $r = 0.61$ m the distance to the

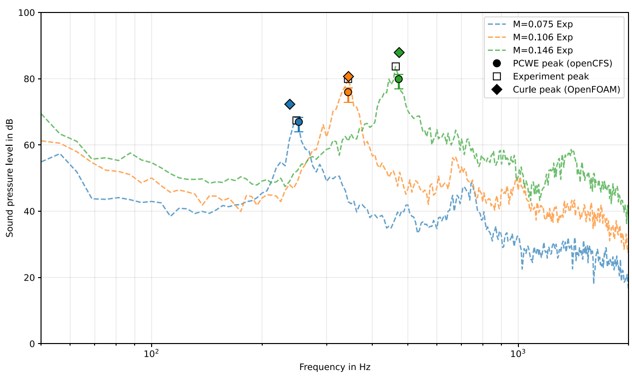

Figure 9. Sound pressure level spectra (ref 20 μPa) obtained for the 20 mm diameter cylinder models in comparison to the aeroacoustic simulation using the PCWE and Curle's analogy.

observer. The third term [36] accounts for the reduced correlation length of the flow structures compared to a fully correlated flow along the cylinder (aspect ratio of 14, see Tab. 2), the correlation length L_c was assumed to be 6 diameters for the shedding frequency. The influence on the SPL peak of the simulation as a result of the spanwise correlation length for a circular cylinder is depicted in the plot. Based on literature, it ranges from $L_c/d \approx 3$ at Re = 43,000 [37] to $L_c/d \approx 5$ at Re = 22,000–48,000 [38, 39] up to $L_c/d \approx 8.2$ at Re = 90,000 [40]. The investigated Reynolds number range is from 30,000 to 70,000. The 3D aeroacoustic simulation using Curle's analogy in OpenFoam is only corrected by the relative correlation length of $5d$ in the simulation compared to $6d$ provided by the literature.

From theory, the acoustic pressure of dipolar sound radiation scales as 2.5 with the Mach number, corresponding to a power of 5 for the acoustic intensity. In 3D, the acoustic pressure scales with the power of 3, defined by the intensity law as a result of Curle's analogy for compact spherical dipoles. From the three 2D simulations, it was found that the data scales with a power of 2.25 with respect to the Mach number. In the experiments, the power-law fit yielded a power of 2.83, which falls between 2D and 3D.

7 Conclusions

A benchmark dataset is presented to improve the open data policy in the acoustic research community. The dataset consists of experimental data and a corresponding numerical simulation setup, implemented in open-source software packages. Both are provided online. The definitions of the geometrical and flow parameters, together with the experimental database, constitute a standardised configuration designated as **FLOW-01**. This configuration is proposed as a validation benchmark for numerical simulation workflows and as a reference standard for the design and calibration of aeroacoustic measurement facilities.

Acknowledgments

The authors thank Stefan Rohark (BTU Cottbus-Senftenberg) for his help with the experimental setup and Alp Biçen (BTU Cottbus-Senftenberg) for his help with the flow measurements.

Funding

S. S. received funding from the COMET project ECHODA ("Energy Efficient Cooling and Heating of Domestic Appliances") under FFG project No. FO999913905. ECHODA is funded within the framework of "COMET – Competence Centers for Excellent Technologies" by BMIMI, BMAW, the province of Styria, and SFG. The COMET program is managed by FFG. S. S. received funding from the FFG under project No. FO999913972.

Conflicts of interest

The authors declare that they have no conflicts of interest in relation to this article.

Data availability statement

The dataset are available in Zenodo, under the reference https://doi.org/10.5281/zenodo.13365560.

References

1. B. Etkin, G.K. Korbacher, R.T. Keefe: Acoustic radiation from a stationary cylinder in a fluid stream (aeolian tones). The Journal of the Acoustical Society of America 29 (1957) 30–36.
2. R.T. Keefe: Investigation of the fluctuating forces acting on a stationary circular cylinder in a subsonic stream and of the associated sound field. The Journal of the Acoustical Society of America 34, 11 (1962) 1711–1714.
3. M.M. Zdravkovich: Flow Around Circular Cylinders: Volume 1: Fundamentals. Vol. 1. Oxford University Press, 1997.
4. M.M. Zdravkovich: Flow Around Circular Cylinders: Volume 2: Applications. Vol. 2. Oxford University Press, 1997.
5. F.V. Hutcheson, T.F. Brooks: Noise radiation from single and multiple rod configurations. International Journal of Aeroacoustics 11, 3, 4 (2012) 291–333.
6. O. Inoue, N. Hatakeyama: Sound generation by a two-dimensional circular cylinder in a uniform flow. Journal of Fluid Mechanics 471 (2002) 285–314.
7. X. Gloerfelt, F. Pérot, C. Bailly, D. Juvé: Flow-induced cylinder noise formulated as a diffraction problem for low mach numbers. Journal of Sound and Vibration 287, 1, 2 (2005) 129–151.
8. K. Karthik, S. Vengadesan, S.K. Bhattacharyya: Prediction of flow induced sound generated by crossflow past finite length circular cylinders. The Journal of the Acoustical Society of America 143, 1 (2018) 260–270.
9. T.F. Geyer: Experimental evaluation of cylinder vortex shedding noise reduction using porous material. Experiments in Fluids 61, 7 (2020) 1–21.
10. E. Sarradj, C. Fritzsche, T.F. Geyer, J. Giesler: Acoustic and aerodynamic design and characterization of a small-scale aeroacoustic wind tunnel. Applied Acoustics 70, 8 (2009) 1073–1080.
11. BASF SE: Basotect – ideal sound absorption and thermal insulation for the transportation industry, 2017. https://download.basf.com/p1/

8a8082587fd4b608017fd64b1e533cf6/en/Basotect%3Csup%3E%C2%AE%3Csup%3E_%E2%80%93_Ideal_Sound_Absorption_and_Thermal_Insulation_for_the_Transportation_Industry_Brochure_English.pdf?view [Accessed: 2026-04-06].
12. T.F. Geyer, A. Lucius, M. Schneider, L. Enghardt: Aerodynamic noise from circular cylinders under turbulent inflow conditions. AIAA Journal 63 (2025) 1–11.
13. R. Porteous, D.J. Moreau, C.J. Doolan: A review of flow-induced noise from finite wall-mounted cylinders. Journal of Fluids and Structures 51 (2014) 240–254.
14. C.-K. Choi, D.-K. Kwon: Wind tunnel blockage effects on aerodynamic behavior of bluff body. Wind and Structures 1, 4 (1998) 351–364.
15. J.B. Barlow, W.H. Rae Jr, A. Pope: Low Speed Wind Tunnel Testing. Vol. 7. INCAS-National Institute for Aerospace Research "Elie Carafoli", 2015.
16. A. Richter, E. Naudascher: Fluctuating forces on a rigid circular cylinder in confined flow. Journal of Fluid Mechanics 78, 3 (1976) 561–576.
17. R.K. Amiet: Refraction of sound by a shear layer. Journal of Sound and Vibration 58, 4 (1978) 467–482.
18. C.L. Morfey, P.F. Joseph: Shear layer refraction corrections for off-axis sources in a jet flow. Journal of Sound and Vibration 239, 4 (2001) 819–848.
19. E. Sarradj: A fast ray casting method for sound refraction at shear layers. International Journal of Aeroacoustics 16, 1, 2 (2017) 65–77.
20. R. Porteous, T.F. Geyer, D.J. Moreau, C.J. Doolan: A correction method for acoustic source localisation in convex shear layer geometries. Applied Acoustics 130 (2018) 128–132.
21. F.E. Jørgensen: How to measure turbulence with hot-wire anemometers: a practical guide. Technical report, Dantec Dynamics, 2001.
22. P. Welch: The use of fast fourier transform for the estimation of power spectra: a method based on time averaging over short, modified periodograms. IEEE Transactions on Audio and Electroacoustics 15, 2 (1967) 70–73.
23. E.A. Dean: Atmospheric effects on the speed of sound. Technical Report ASL-CR-79-0100-4, US Army Electronics Research and Development Coimmand, 1979.
24. S. Schoder, M. Kaltenbacher: Hybrid aeroacoustic computations: state of art and new achievements. Journal of Theoretical and Computational Acoustics 27, 4 (2019) 1950020.
25. M. Kaltenbacher, K. Roppert, S. Schoder, J. Heinz: Stable finite element formulation for the perturbed convective wave equation. IIb 1, c2 (2021) c2.
26. S. Schoder, K. Roppert: openCFS: open source finite element software for coupled field simulation – Part acoustics. Preprint arXiv:2207.04443, 2022.
27. S. Schoder: openCFS-data: implementation of the stochastic noise generation and radiation model (SNGR). Preprint arXiv:2302.05622, 2023.
28. S. Schoder: Offline coupling of segregated multi-physical simulations with consistent boundary conditions and source terms based on scattered data. Preprint arXiv:2308.04608, 2023.
29. P. Maurerlehner, S. Schoder, J. Tieber, C. Freidhager, H. Steiner, G. Brenn, K.-H. Schäfer, A. Ennemoser, M. Kaltenbacher: Aeroacoustic formulations for confined flows based on incompressible flow data. Acta Acustica 6 (2022) 45.
30. S. Schoder, A. Wurzinger, C. Junger, M. Weitz, C. Freidhager, K. Roppert, M. Kaltenbacher: Application limits of conservative source interpolation methods using a low mach number hybrid aeroacoustic workflow. Journal of Theoretical and Computational Acoustics 29, 1 (2021) 2050032.
31. S. Schoder, A. Wurzinger: Dataset CYLinCF-01 creation pipeline: circular cylinder in a crossflow, Mach Number 0.03 and Reynolds Number 200. Preprint arXiv:2303.05265, 2023.
32. S. Schoder, K. Roppert, M. Weitz, C. Junger, M. Kaltenbacher: Aeroacoustic source term computation based on radial basis functions. International Journal for Numerical Methods in Engineering 121, 9 (2020) 2051–2067.
33. S. Schoder, P. Maurerlehner, A. Wurzinger, A. Hauser, S. Falk, S. Kniesburges, M. Döllinger, M. Kaltenbacher: Aeroacoustic sound source characterization of the human voice production-perturbed convective wave equation. Applied Sciences 11, 6 (2021) 2614.
34. OpenCFD Ltd. OpenFOAM User Guide: Post-processing Noise. ESI Group, Bracknell, UK, 2024. Version v2406. https://www.openfoam.com/news/main-news/openfoam-v2406.
35. Newby Curle: The influence of solid boundaries upon aerodynamic sound. Proceedings of the Royal Society of London. Series A. Mathematical and Physical Sciences 231, 1187 (1955) 505–514.
36. C. Kato, A. Iida, Y. Takano, H. Fujita, M. Ikegawa: Numerical prediction of aerodynamic noise radiated from low mach number turbulent wake, in: 31st Aerospace Sciences Meeting, 1993, p. 145.
37. S. Szepessy: On the spanwise correlation of vortex shedding from a circular cylinder at high subcritical Reynolds number. Physics of Fluids 6, 7 (1994) 2406–2416.
38. D. Casalino, M. Jacob: Prediction of aerodynamic sound from circular rods via spanwise statistical modelling. Journal of Sound and Vibration 262, 4 (2003) 815–844.
39. M.C. Jacob, J. Boudet, D. Casalino, M. Michard: A rod-airfoil experiment as a benchmark for broadband noise modeling. Theoretical and Computational Fluid Dynamics 19, 3 (2005) 171–196.
40. R. Orselli, J. Meneghini, F. Saltara: Two and three-dimensional simulation of sound generated by flow around a circular cylinder, in: 15th AIAA/CEAS Aeroacoustics Conference (30th AIAA Aeroacoustics Conference), 2009, p. 3270.

Cite this article as: Geyer T.F. Abromeit P. & Schoder S. 2026. *FLOW-01*: A benchmark dataset for aerodynamic noise and wake flow fields generated by circular cylinders in a crossflow. Acta Acustica, **10**, 74. https://doi.org/10.1051/aacus/2026068.